The CathPilot: A Novel Approach for Accurate Interventional Device Steering and Tracking

James J. Zhou, Amaar Quadri, Alykhan Sewani, *Member, IEEE*, Yara Alawneh, Rene Gilliland-Rocque, Christopher Magnin, Andrew Dueck, Graham A. Wright, and M. Ali Tavallaei, *Member, IEEE*

***Abstract*—Accurate device navigation and control are significant challenges in various minimally invasive cardiovascular interventions. The long length of the devices used (e.g., catheters and guidewires), their high flexibility, and their engagement with the tortuous anatomy limit the accurate and reliable control and navigation of the device's tip. This article aims to design, develop, and assess a novel alternative solution that promises to overcome the major limitations of conventional devices. By utilizing an expandable cable-driven mechanism and a corresponding 3-D cam surface for cable length adjustment, we propose a fully manually operated system that can be navigated through the tortuous anatomy and then teleoperated to allow for accurate, reliable, and localized position control and tracking of the device. In this article, the methods of design, development, and verifications of this system are presented. The system's performance is assessed under different path tortuosity conditions and different opening diameters of the expandable frame. Our results indicate that the proposed system provides complete teleoperation of the device within the full reachable workspace of the mechanism and allows for positioning and tracking of the device with submillimeter accuracy irrespective of the tortuosity of the path and expansion size of the frame. *Ex-vivo* phantom model experiments also show the device significantly outperforms conventional devices in terms of navigation time and success rate. The CathPilot allows for direct manipulation, accurate positioning, and tracking of the device tip relative to the anatomy, promising to overcome some of the major limitations of conventional interventional devices.**

***Index Terms*—Cable-driven parallel manipulator/mechanism, cable-driven robotics, cardiovascular interventions, minimally invasive interventions, steerable catheter.**

I. Introduction

CARDIOVASCULAR diseases continue to be the leading cause of death and short- and long-term disability [1], [2]. The primary surgical interventions for diagnosis, management, and treatment of cardiovascular disease are minimally invasive catheter-based procedures, which have been rapidly adopted globally. Today, more than ten million catheter-based cardiovascular interventions are performed worldwide each year [3]. However, despite their many benefits, many such catheter-based procedures continue to suffer from extremely high failure rates—above 20% for some procedures [4]–[6], long procedure times, and alarming complication rates (up to 30% for many commonly performed procedures) [7]–[9]. These factors ultimately risk patient lives and create significant undesired social and economic burdens.

Conventional catheter-based cardiovascular interventions typically use nonsteerable or cable-actuated steerable catheters. These long and flexible devices are passive and manually manipulated from outside the patient body. In such procedures, accurate and reliable navigation and control of the device tip relative to the anatomy is extremely challenging [10], [11]. Two contributors to this limitation include: First, the devices are soft and compliant and have unpredictable interactions with the cardiovascular anatomy along their path; and second, the procedures are typically guided with 2-D projection X-ray imaging that fails to provide 3-D anatomical information and depth perception. Both Awaz *et al.* and Hu *et al.* provide detailed literature surveys of steerable catheters and highlight their limitations in precise device positioning and navigation [11], [12]. In [13], the effects of such constraints on the reachable workspace and deliverable forces for conventional devices have been characterized. We believe these limitations—that have not been fully addressed by conventional steerable catheters—ultimately contribute to long procedure times and extended radiation exposure to the patient and health care team, as well as high failure and complication rates.

Manuscript received 25 December 2021; revised 8 April 2022 and 26 May 2022; accepted 2 July 2022. Date of publication 27 July 2022; date of current version 14 December 2022. Recommended by Technical Editor Z. Xia and Senior Editor G. Alici. This work was supported in part by the Ontario Research Fund, Toronto Metropolitan University (formerly Ryerson University), in part by the National Sciences and Engineering Research Council of Canada, and in part by the Canada Research Chair program. *(Corresponding author: M. Ali Tavallaei.)*

James J. Zhou, Alykhan Sewani, Yara Alawneh, Rene Gilliland-Rocque, and M. Ali Tavallaei are with Toronto Metropolitan University, Toronto, ON M5B 2K3, Canada (e-mail: ali.tavallaei@ryerson.ca; alykhan.sewani@ryerson.ca; yara.alawneh@ryerson.ca; rene.gillilandrocque@ryerson.ca; atavallaei@gmail.com).

Amaar Quadri is with the University of Waterloo, Waterloo, ON N2L 3G1, Canada (e-mail: aquadri@uwaterloo.ca).

Christopher Magnin is with the Magellan Biomedical Inc., Richmond Hill, ON L4C 5X4, Canada (e-mail: christopher.magnin@gmail.com).

Andrew Dueck and Graham A. Wright are with Sunnybrook Research Institute, Toronto, ON M4N 3M5, Canada, and also with the University of Toronto, Toronto, ON M5S 1A1, Canada (e-mail: andrew.dueck@sunnybrook.ca; graham.wright@sunnybrook.ca).

This article has supplementary material provided by the authors and color versions of one or more figures available at https://doi.org/10.1109/TMECH.2022.3188955.

Digital Object Identifier 10.1109/TMECH.2022.3188955

This work is licensed under a Creative Commons Attribution-NonCommercial-NoDerivatives 4.0 License. For more information, see https://creativecommons.org/licenses/by-nc-nd/4.0/

There are many cardiovascular interventions that could benefit from more accurate and reliable device navigation and tracking. Examples include gate cannulation in endovascular aneurysm repair procedures that suffer from very long procedure times (up to 8 h) [14], [15]; coronary sinus cannulation in cardiac resynchronization therapy; accurate needle positioning and steering for procedures, such as transseptal puncture [16] or cardiac drug delivery and regenerative therapy [17], [18]. However, in this article, we will primarily focus on an example application of the proposed technology in arterial revascularization in patients with peripheral arterial disease (PAD) and critical limb ischemia. PAD affects 12–14% of the general population in North America alone [19], [20]. Unfortunately, PAD is associated with significant morbidity and mortality. The prime surgical approach for the management of PAD is through endovascular revascularization. However, many such procedures immediately fail (up to 30%), merely for technical reasons and the inability of the interventionalist to *"cross"* the occlusion with the guidewire [4], [21], [22]. These failures are despite the presence of microchannels as well as soft penetrable segments within the arterial occlusions [23]–[25] and, hence, calling for improved methods and solutions.

To address some of the limitations of conventional catheter navigation, active electromechanical telerobotic catheter navigation platforms have also been developed [26]. These solutions primarily allow the user to perform the procedure remotely, far from the ionizing radiation of the X-ray source. The prime technology that is used in such systems is cable-actuated backbone-based structures. Alternatively, there is also extensive research activity on concentric tubes, as well as soft, hydraulic-based robotic systems [27], [28]. A major common challenge to all such designs can be attributed to limitations imposed by the system and vessel interactions and the long, tortuous navigation path and remote mechanical manipulation from outside the body that ultimately affect the device's performance and limit its reachable workspace, accuracy, and force delivery [10], [13]. These technologies do not address the lack of 3-D visualization that exists with conventional image-guidance techniques, such as projection X-ray fluoroscopy.

Electromagnetic catheter navigation systems are also commercially available that address this problem directly, a commercial example being the Stereotaxis Niobe system [29]. They allow for direct magnetic manipulation of custom devices with integrated magnets at their tip. This method allows for direct manipulation of the device tip, mostly independent of the mechanical engagements between the catheter shaft and the tortuous anatomy along its length. Therefore, it allows for more accurate and direct device steering and navigation [29]. However, these systems are relatively expensive to purchase, install, and operate, as they require expensive custom devices, large adjustable magnetic field sources, and a dedicated room. In addition, these systems manipulate and track the device relative to the geometric coordinates of the electromagnetic source outside of the patient body. Therefore, manipulation and tracking are not relative to the anatomy but rather to the source of manipulation outside the patient body [11], [30].

To address the challenges associated with device visualization and tracking, various sensing techniques, such as electromagnetic-based tracking and fiber optic sensing (e.g., fiber Bragg grating) have been used [31], [32]. One of the limitations of such sensing technologies is that they require costly custom devices with integrated sensors (e.g., electromagnetic coils). Also, the tracking of such devices is also performed relative to the tracking system's coordinates rather than the moving anatomy itself, which is what is of interest.

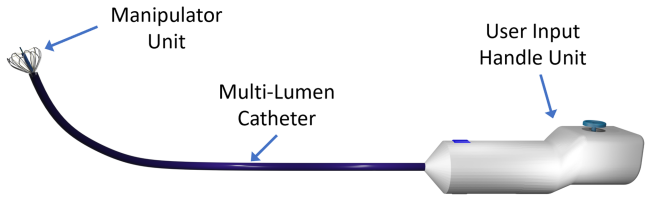

Fig. 1. Representative CAD model of the CathPilot is shown with its three main subcomponents: the manipulator unit, the multilumen catheter, and the user input handle unit.

It is our goal to develop a comprehensive solution that addresses the fundamental limitations in steering, tracking, and navigation of conventional steerable catheters. Our proposed solution draws inspiration from cable-driven parallel mechanisms (CADPAM; also referred to as CDPMs).

Unlike conventional robots with rigid links, CADPAMs utilize cables attached to the end-effector to create motion. They provide many advantages over rigid-link mechanisms, such as a larger workspace, a higher payload-weight ratio, and low manufacturing and assembly costs. Given these advantages, there have been great achievements in the design, modeling, and control of cable-driven robots [33]–[36]. Conventional CADPAMs require a rigid frame or structure to provide leverage points for the cables and to act as a geometric reference for the system. However, the large size of these frames hinders their use for applications where region access is limited due to size constraints.

We propose to use an e**x**pandable-CADPAM (X-CADPAM), which utilizes a self-expandable frame that can be contracted (e.g., within a constraining outer sheath) or deployed as needed. As has been described in [37]–[39], an expandable frame approach permits travel through a narrow passageway to reach the target area. Once at the desired location, the frame is then expanded (e.g., by retracting the outer sheath). This approach allows us to take advantage of the specific benefits of CADPAMs while overcoming their challenges due to their frame size, which limits their mobility and applications for use in constrained environments. This article describes the design, development, verification, and *ex-vivo* validation of a purely passive teleoperated version of a self-deployed X-CADPAM system for potential applications in minimally invasive interventions. We call this system the *CathPilot*.

II. Design and Modeling

The CathPilot (see Fig. 1) consists of two main system components: the manipulator unit; and a user input handle unit. The handle allows for remote manual actuation of the manipulator. The design and development of each of these system components are described in detail in this section.

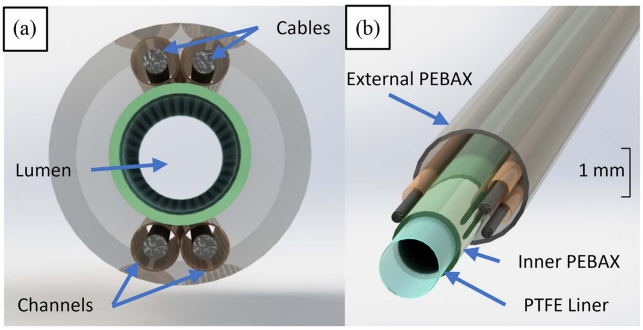

Fig. 2. Key component layers of the multilumen catheter. (a) Cross section of the catheter indicating the cable routing with respect to the catheter lumen. (b) Each individual layer in the catheter's construction.

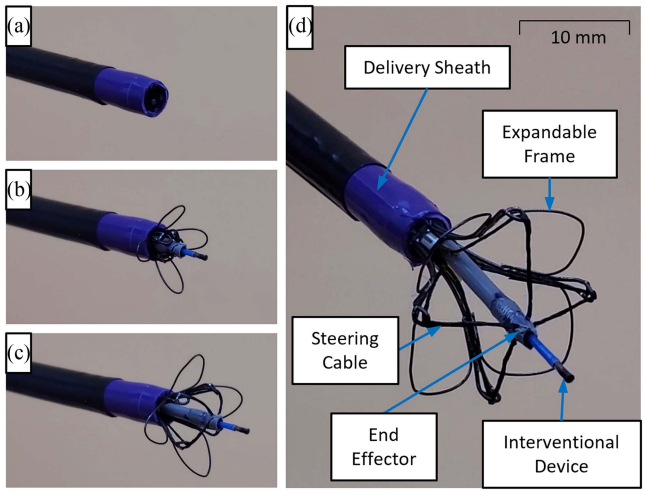

Fig. 3. (a) Expandable frame of the CathPilot fully contained within the delivery sheath. (b) and (c) Expandable frame being gradually extracted and expanded toward full expansion. (d) Frame fully expanded and identifies the various components of the manipulator.

A. Manipulator Unit

The manipulator, as shown in Fig. 1, is comprised of an expandable frame, four cables, and an end-effector (i.e., an internal catheter). A 70-cm multilumen catheter is used to connect the input handle to the manipulator. This catheter has five polytetrafluoroethylene (PTFE) coated channels that are covered with PEBAX. Four of these channels each support one of four PTFE cables (O.D. 0.012") that pass from the handle to the manipulator, whereas the fifth larger lumen, with a PTFE liner, is reserved for the main interventional device, which the user intends to steer and track and continues throughout the device and exits at the rear end of the handle. A cross section of the multilumen catheter design is shown in Fig. 2. We quantified the elasticity of the PTFE braided cables used. The Young's modulus was found to be 120 GPa. Based on our experiments, the maximum force required to overcome the friction in the system and move the end-effector to the extremity of the frame is 1.2 N for all three tested configurations. Assuming a conservative cable length of 1 m, the amount of strain for this tension level would be less than 1.5×10^{-8} m, hence the elasticity effects have been ignored.

The expandable frame is a critical component of our proposed system. We set following four main design requirements for this frame.

1) The frame must be deliverable through a 12Fr sheath (inside diameter) with an outer diameter of 5.3 mm.
2) The frame must be able to expand to a maximum diameter of 20 mm when the outer constraining sheath is removed.
3) The frame must be able to maintain its shape and relative rigidity when under stress due to the tension of the cables as the manipulator is operated.
4) It must provide four anchor points for the four cables used.

Given the multiple potentially conflicting design requirements, we used an iterative design approach to achieve a working solution. We leveraged finite element analysis in Ansys 2021(Ansys, Canonsburg, PA, USA) to analyze the maximum loading condition of collapsing the frame under the sheath—with various frame shapes and thicknesses—using the Von Mises yield criterion. After multiple design iterations, implementations, and testing, we achieved the design shown in Fig. 3 that met the specified design requirements. This design consists of eight different segments made of Ni–Ti wires of 0.010–0.015" diameter, which was shape-set using custom-designed steel die. The segments were heat-treated at 475 °C for 15 min and then quenched immediately in room temperature water. Ultimately, the NiTi segments were welded using a laser welder (Select, Coherent Rofin) onto a 304 stainless steel hypotube of 0.12" O.D. and 0.0035" wall thickness. The hypotube was then adhered to the multilumen catheter.

As described, our proposed X-CADPAM supports four cables to actuate the end-effector. Therefore, the system is redundantly constrained for motion in 2-D. While the minimum number of required cables is three, the use of only three cables leads to a much smaller triangular workspace compared to the square workspace achievable with four cables. Further addition of cables will further increase the workspace area, however, at the cost of the increased complexity of the device.

B. User Input Handle Unit (Master)

The handle unit is designed to permit remote operation of the device with a purely passive design, actuated with the user's manual input energy. This approach allows us to avoid the safety concerns associated with active and motorized designs, which add to the challenge of achieving regulatory approval. Furthermore, this permits cost reduction by eliminating the need for motors, sensors (e.g., position, tension), and corresponding drivers and control units.

As the CathPilot has 2 DOF and utilizes four cables in a redundantly constrained configuration, all four cables must be manipulated simultaneously to eliminate their slack and adjust their tension. In the proposed passive mechanism, all four cables require simultaneous adjustment by the user. For an ergonomic solution, the user/interventionalist must operate the CathPilot with one hand, as they need the other hand to be free for manipulation of the primary interventional device (e.g., guidewire

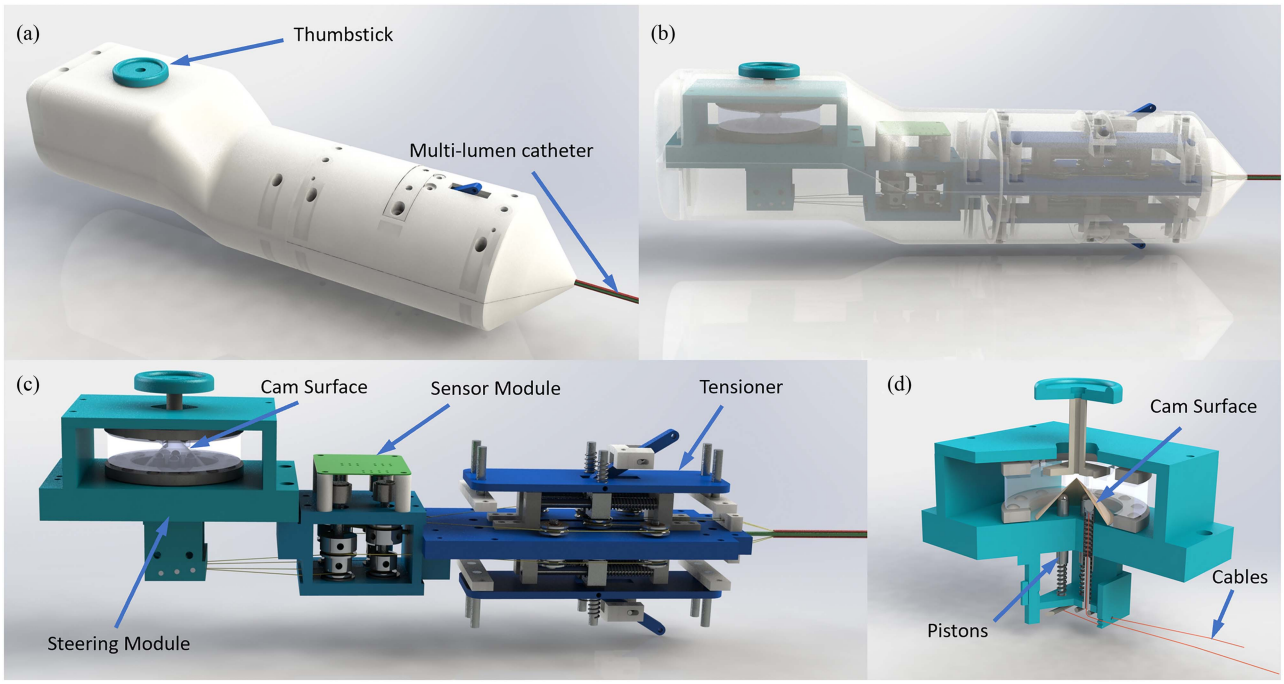

Fig. 4. User input handle unit is shown. (a) Left-handed handle unit and the user thumbstick interface. (b) Handle with a semitransparent shell. (c) Internal mechanisms of the handle and various subsystems. (d) Steering module consisting of the 3-D cam surface (with a cross-sectional cut), pistons as cam-followers, and corresponding cables and their location within the pistons.

or catheter) that is inserted and steered, and tracked by the CathPilot. The requirement for simultaneous adjustment of the four cables to achieve position control in a 2-DOF space with an ergonomic yet manually operated user interface creates specific engineering challenges that require a novel solution.

We propose the design of a 3-D cam and cam follower system to map the manipulator workspace to that of the master input unit through adjustments of cable lengths. This approach permits simultaneous adjustment of the four cable lengths to maintain their desired set tension. In other words, the steering of the manipulator is achieved by using a 3-D cam surface [see Fig. 4(c) and (d)] acting as the master input unit that can be translated with 2 DOF in a planar fashion. The motion of the cam surface in the 2-D plane is scaled and mapped directly to the motion of the manipulator unit.

In our proposed 3-D cam system, the cables are mechanically coupled to the cam-followers, which are spring-loaded pistons. This ensures that cam followers continue to maintain contact with the cam profile [see Fig. 4(d)]. As the cam surface translates in 2-D, the variation in the height of the profile at each piston location limits the height of each piston and, therefore, the displacement of the corresponding cable connected to it [see Fig. 4(c) and (d)]. By proper calculation of the shape of the cam surface profile, we can adjust the lengths of all the cables in proportion and achieve a linear mapping between the position of the cam surface and the end-effector of the manipulator unit, allowing us to attain manual teleoperation of the system.

To calculate the required shape of the cam, we assume that after full expansion, the frame maintains its rigidity during device operation. We also assume that the four anchor points

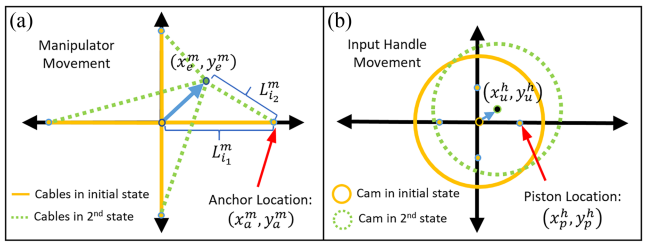

Fig. 5. (a) Schematic showing the position of the end-effector and cable lengths in the manipulator coordinate frame (catheter unit). (b) Schematic showing the corresponding position of the cam surface unit in the user input (master) coordinate frame.

on the frame, as well as the positions of the four pistons in the master unit, each correspondingly form a square shape (see Fig. 5). We assume the origin of the coordinate system of both the input unit and the manipulator unit to be at the center of the square workspace. Let (x_a^m, y_a^m) define the coordinates of one of the anchor points in the manipulator coordinate system, as shown in Fig. 5(a), where the subscript "a" refers to the anchor point, and superscript "m" refers to the corresponding frame of reference, in this case being the manipulator coordinate system. Let (x_p^h, y_p^h) define the coordinates of one of the pistons in the input handle unit coordinate system, as shown Fig. 5(b), where superscript "h" refers to the handle and the "subscript "p" refers to the piston. Both of these positions are constants. The two moving components are the manipulator end-effector position $(x_e^m, y_e^m)$and the displacement of the handle cam surface $(x_c^h$

,y_c^h). Note that subscripts "*e*" and "*c*" refer to end-effector and cam surface correspondingly.

As the end-effector moves, the change in length of one of the cables on the manipulator side that is anchored to the point (x_a^m, y_a^m) is the length of the vector from that anchor point (x_a^m, y_a^m) to the end-effector position (x_e^m, y_e^m). To simplify the calculations, we assume a 2-D workspace for the end-effector with a starting initial condition of $(x_e^m = 0,\ y_e^m = 0)$ and a final point at (x_e^m, y_e^m). The change in length of the *i*th cable can be calculated as follows:

$$\Delta L_i^m = L_{i_2}^m - L_{i_1}^m = \sqrt{(x_a^m - x_e^m)^2 + (y_a^m - y_e^m)^2} - \sqrt{x_a^{m2} + y_a^{m2}}. \tag{1}$$

On the input handle side, the cables are individually constrained to the cam surface at fixed positions. Based on our assumption, these four positions resemble the same square shape formed by the anchor point positions in the manipulator. The cam surface is constrained to move in a plane with 2 DOF. The cables are passed through pistons that can move linearly and perpendicular to the $x^h - y^h$ plane at the input handle side [see Fig. 4(d)]. Springs within each piston ensure that the pistons are always pushing against the cam surface. Therefore, the length of the cables within the pistons are constrained by the cam surface height at the corresponding piston location. Therefore, the variable length of each cable is determined by the variation in the height of the cam surface at the corresponding piston position. The variation in the length of the *i*th cable can be calculated by finding the difference between the initial height of the cam surface at that particular coordinate of the *i*th piston $(x_{p_i}^h, y_{p_i}^h)$ as the cam surface is shifted on the $x^h - y^h$ plane or, in other words, the variations of z_i^h.

The cam surface at the input handle is described as a function of (x^h, y^h). We assume that the cam surface is restricted to move only in the 2-D $x^h - y^h$ plane. We also assume that the user actuates this surface by moving the center of the cam surface to a particular point on the control handle (x_u^h, y_u^h) with an initial starting point of $(x_u^h = 0,\ y_u^h = 0)$. Starting from the origin (at the center of the square formed by the pistons) to a new position in the plane, the change in the height of the cam surface—and therefore the change in the length of the corresponding *i*th cable at the master side or ΔL_i^h — at the *i*th piston position is

$$\Delta L_i^h = z\left(x_{p_i}^h - x_u^h, y_{p_i}^h - y_u^h\right) - z\left(x_{p_i}^h, y_{p_i}^h\right) \tag{2}$$

where $(x_{p_i}^h, y_{p_i}^h)$ is the position of the ith piston, in the handle coordinates and z(x^h, y^h) is the height of the cam surface as a function of the coordinates (x^h, y^h). We define a ratio factor $r \equiv$ ratio to represent the ratio between the dimension of the expandable frame anchor coordinates and the four pistons in the master unit. In other words

$$\left(r\left|x_{p_i}^h\right|, r\left|y_{p_i}^h\right|\right) = \left(\left|x_a^m\right|, \left|y_a^m\right|\right). \tag{3}$$

We wish to solve for the cam surface z(x^h, y^h) such that the input motion on the cam surface is a proportionally scaled replica of the end-effector motion with a ratio of *r*. In other words, we would like to find the solution for the surface z such that the vector (rx_u^h, ry_u^h) is a replica of (x_e^m, y_e^m). We assume negligible cable elasticity and that the actuation of the surface z leads to a direct linear relationship between the change in the cable lengths occurring at the handle input and manipulator

$$\alpha\Delta L_i^h = -\Delta L_i^m \text{ or } \Delta L_i^h = -\frac{1}{\alpha}\Delta L_i^m \tag{4}$$

where α is a constant reflecting the ratio of the corresponding cable length changes between the hand input and the manipulator. We can now rewrite (2) as

$$z\left(x_{p_i}^h - x_u^h, y_{p_i}^h - y_u^h\right) - z(x_{p_i}^h, y_{p_i}^h = -\frac{1}{\alpha}\sqrt{(x_a^m - x_e^m)^2 + (y_a^m - y_e^m)^2} + \frac{1}{\alpha}\sqrt{x_a^{m2} + y_a^{m2}}. \tag{5}$$

In our application, the location of the *i*th piston at the handle input $(x_{p_i}^h, y_{p_i}^h)$ and the position of the anchors at the manipulator (x_a^m, y_a^m) are arbitrary. Therefore, we can assume a common virtual coordinate for both the handle input and the manipulator where both $x - y$ coordinates are aligned and overlap. With the assumption given by (3), and assuming the goal of $(rx_u^h, ry_u^h) = (x_e^m, y_e^m)$, we can rewrite (5) within this common coordinate

$$z\left(x_i - x_u, y_i - y_u\right) - z\ (x_i, y_i) = -\frac{1}{\alpha}\sqrt{(rx_i - rx_u)^2 + (ry_i - ry_u)^2} + \frac{1}{\alpha}\sqrt{r^2x_i^2 + r^2y_i^2}. \tag{6}$$

We see that a unique solution to (6) is

$$z\ (x, y) = H_0 - \frac{r}{\alpha}\sqrt{x^2 + y^2} \tag{7}$$

where H_0 is a constant that can be arbitrarily selected as required (e.g., based on the ergonomic requirements for the input handle). For the sake of simplicity, we can assume that $\alpha = r$. This results in a cone with a slope of 1

$$z\,(x, y) = H_0 - \sqrt{x^2 + y^2}. \tag{8}$$

In the case where $r \neq 1$, if we desire to use the same cone with a slope of 1, we can still obtain the desired one-to-one motion by utilizing a gear ratio on the corresponding cables such that $\Delta L_i^m = r\Delta L_i^h$.

Utilizing the proposed calculated cam surface, we can achieve a purely passive teleoperated system that allows remote controlling of the end-effector by manipulating the user handle input cam surface with 2 DOF. This approach will enable us to adjust the length of all cables simultaneously without needing an active control loop with sensors and actuators to sense the master input and control the position of the manipulator unit.

C. Tensioner

The proposed system is designed to operate up to a maximum frame expansion size of 20 mm. While each cable length can be adjusted for perfect operation with the 3-D cam surface as the system is manipulated, at smaller expansion sizes of the frame, there would be cable sagging, and all cable lengths need to be shortened proportional to the frame size reduction. To

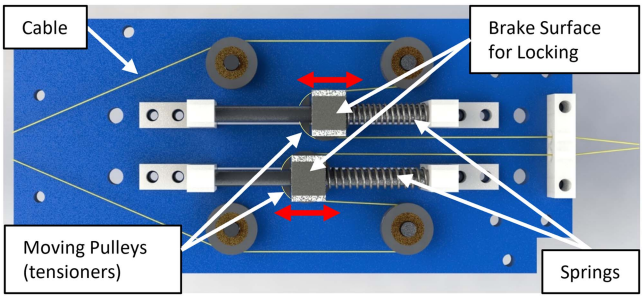

Fig. 6. Top view of the tensioner showing the spring-loaded pulley movement that accounts for cable-sagging and overtensioning. Red arrows indicate direction of motion of moving pulleys (tensioners).

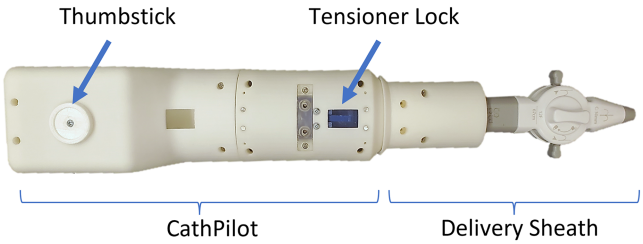

Fig. 7. CathPilot handle prototype coupled to a conventional 12 Fr delivery sheath is shown. The delivery sheath is free to move axially or radially relative to the CathPilot. See supplemental media file for more information.

accommodate various sizes of the expandable frame, we propose the use of a tensioner that can passively release and withdraw all cables simultaneously depending on the opening size.

The tensioner mechanism is used only when the expansion size of the manipulator frame changes to adjust all cable lengths by the same amount simultaneously and absorb cable sagging. Four spring-loaded pulleys accommodate any required change in the cable lengths (see Fig. 6); they are then locked in place with a self-locking brake to avoid affecting the device's performance during steering and tracking. When unlocked, the tensioner springs merely absorb the cable sagging. The tensioner lock is then applied during runtime. Therefore, a minimum spring constant is needed for the tensioner springs. We used off-the-shelf springs that could accommodate 6.5 mm of motion and had an unloaded length of 0.938" (23.8 mm) and a spring constant of 0.24 lb/in (0.042 N/mm). The corresponding CathPilot handle prototype, which contains all the previously described subcomponents, is shown in Fig. 7.

D. Real-Time Position Tracking

By using the X-CADPAM concept in our proposed CathPilot system, we can track the position of the manipulator's end-effector relative to the frame in real time. This can be achieved by using the observable variations of the four cables within the device handle to estimate the end-effector position in the expanded frame. The expandable frame anchors onto the local anatomy (similar to a stent) and provides both a mechanical reference for manipulation and a geometrical reference for measurement of the device's position relative to the tissue to which it is anchored. This is particularly valuable in minimally invasive interventions, as it allows the user to see where they are or have been relative to the anatomy of interest. While X-ray fluoroscopy provides projection images that provide 2-D information of the device position without depth information, the CathPilot frame can be easily deployed such that its workspace is perpendicular to the X-ray plane, or the X-ray beam can be oriented to achieve the same. Therefore, the CathPilot tracking within its plane provides the missing depth information allowing the user to have full 3-D visualization of the device and, most importantly, relative to the anatomy of interest to which the frame is anchored. The potential advantage to the end-user is seeing where they are and recording where they have been to help reduce the random trial and error approach and to help reduce procedure time and failure rates.

For measurement, we coupled a 14-b magnetic rotary position sensor (AS5048B, AMS AG, Premstätten, Austria) to each of the four cables, as is shown in Fig. 4(c). In this arrangement, the displacement of each cable leads to the rotation of a corresponding shaft that is then measured with the rotary position sensor.

Under ideal circumstances, the calculations for position estimation would have been straightforward. Assuming a perfect planar workspace, one can calculate the position of the end-effector by calculating the intersection of the two circles with centers about the two anchor positions with radii equal to the cable lengths, which is obtainable from the cable position sensors. However, our initial assessments revealed that this approach yields poor tracking performance, possibly due to multiple model uncertainties including: the deflection of the expandable frame and uncertainty in the anchor positions; nonlinear friction between the cable and the system; nonlinear friction between the cam and the pistons; nonlinearity of the springs; and a nonplanar workspace of the manipulator.

Due to multiple contributing factors to the model uncertainty, we chose to use a machine learning approach to establish a relationship between the observed cable length variations as input and the end-effector position as output. For obtaining our training dataset, we developed the setup shown in Fig. 8(a). To control the expansion sizes of the frame, we 3-D printed fixtures [see Figs. 8(a) and 9(b)] for the frame at four different sizes of 10, 12.5, 15, and 17.5 mm.

To measure the actual position of the end-effector, we used a calibrated camera. The camera was equipped with a variable focal length (2–50 mm) and uses the IMX322 sensor (Sony, Tokyo, Japan). Fiducial markers on the fixture with known geometry and positions were used for camera calibration and accurate measurement of the end-effector position relative to the horizontal and vertical axes of the expandable frame, as is shown in Fig. 9(b).

For the machine learning algorithm, we assumed four different models to be trained, one for each of the chosen expansion sizes. At each expansion size, we obtained 2000 points of data with four features (one for each cable length) to train the corresponding models. We selected a support vector regression model, provided by scikit-learn [40], using the radial basis

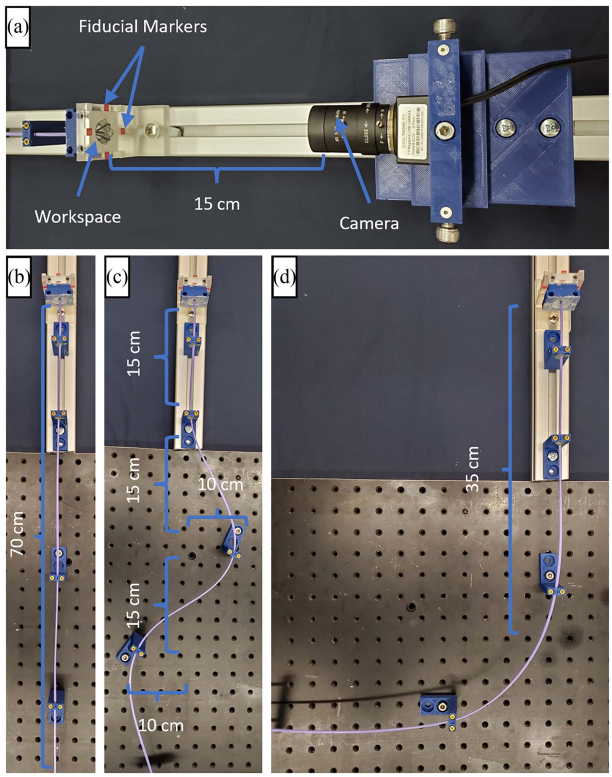

Fig. 8. Setup for accuracy assessment experiments is shown. (a) Position of the manipulator relative to the camera for measurement of the actual position. (b) Catheter in the straight configuration. (c) Catheter in the S shape configuration. (d) Catheter in the 90° bend configuration.

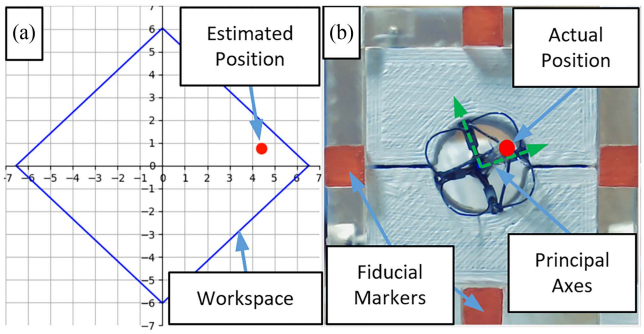

Fig. 9. Estimated tracked position in the GUI and the ground reference from the camera stream images are shown. (a) GUI with the device workspace and real-time estimated position. (b) Camera stream images used to measure the actual positions (the corresponding frame of reference for these measurements is also shown).

function kernel with a gamma of 0.25 and an L2 regularization parameter coefficient, C, of 1.0.

To apply the trained models for estimation of the end-effector position, initially, we need to determine which model, or weighted combinations thereof should be used in the particular arrangement based on the expanded size of the manipulator. To determine this, the user was asked to move the input handle thumbstick to the four extreme corners of the workspace (up/down and left/right) to obtain the maximum variations on each of the four cables. Based on the mean of the maximum cable length variations, the closest corresponding model size was identified. As the user moves the thumbstick within the maximum range of the input, the cam follower piston has reached the maximum retractable cable length, will no longer have contact with the surface and, hence, will not vary anymore, which is detected using the rotary position sensors.

III. Verification and Validation

A. Verification Experiments

With the coordinates output from the tracking algorithm, we designed a graphical user interface (GUI), using Python's Tkinter library, to output the estimated position of the end-effector with respect to the estimated size of the frame [see Fig. 9(a)]. Using the same camera arrangement for measurement of the actual position of the end-effector, we compared the estimated positions of the end-effector to the measured positions. As it is essential to assess the effect of the passage path and shape of the catheter on tracking, we tested the device in three different configurations, including straight, S shaped, and 90° bend. For each configuration, we assessed performance at the four different expansion sizes. For each of the 12 experiments, we acquired approximately 30 points in the workspace and calculated the error between the estimated positions and the ground truth obtained from the camera image stream. These errors at the various locations were also interpolated and plotted to generate corresponding error heatmaps for each catheter shape and frame expansion size. While the training expansion sizes were sparse and were merely for demonstration purposes, the set can be easily increased to include more training sets with finer increments in sizes. However, to show the robustness of the system, we also assessed the tracking algorithm with the frame expanded to untrained intermediate sizes of 11.25, 13.75, and 16.25 mm by averaging the position estimates from the nearest trained size models. Furthermore, to demonstrate the robustness of tracking algorithm to the various unseen configurations of the catheter during training, we used a leave one out approach, where the data from two configurations (i.e., selected from straight, S bend, and 90° bend) were used for training and then assessments were made of the tracking algorithm performance using the third left out configuration. This was repeated for all three configurations, each at sizes of 10, 12.5, 15, and 17.5 mm.

While the user would be relying on the estimated position from the cable length variations (i.e., provided to them in the graphic user interface shown in Fig. 9), which was assessed as described, it is also of value to analyze the error between the mapping from the thumbstick at the handle and the end-effector. For this purpose, a camera was mounted on top of the thumbstick such that the shaft was exposed to facilitate accurate optical tracking of the thumbstick planar (x, y) position. The corresponding position of the end-effector was measured with the same method described previously, with more than 20 points acquired in the workspace at each expansion size (10, 12.5, 15, and 17.5 mm) in all three catheter configurations.

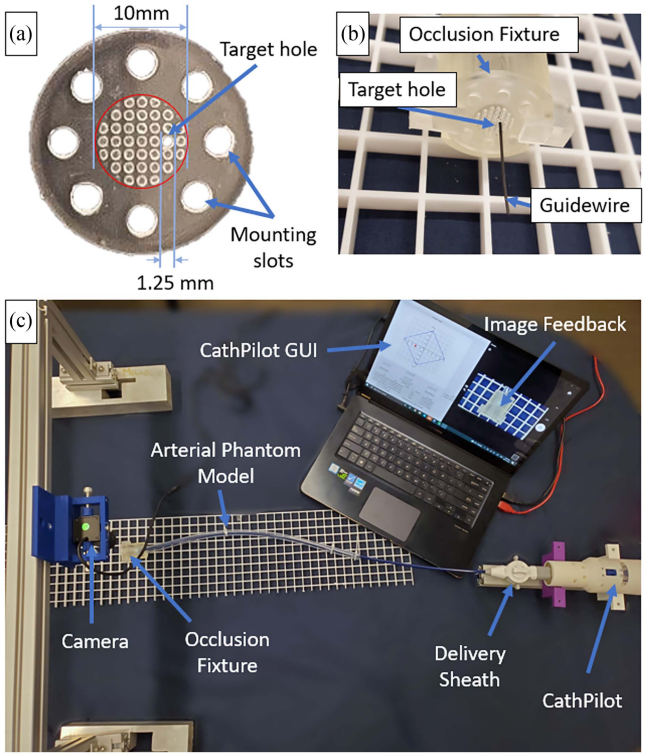

Fig. 10. Phantom model and the corresponding validation experiment setup are shown. (a) One of the four occlusions with a penetrable 1.25-mm target hole within an array of dead-end dimples; the I.D. of the tube artery model matches the dimpled area indicated with the red circle. (b) Semitransparent fixture for holding the occlusion and shows a guidewire that has passed through the target hole. (c) Setup, including the flexible arterial phantom model connected to the occlusion fixture, as well as the camera mimicking conventional X-ray fluoroscopy and providing top-view image feedback. The CathPilot, its delivery sheath, and its GUI are also shown.

B. Application of CathPilot for Lesion Crossing: Phantom Validation Experiments

We propose the first application example of the CathPilot for endovascular revascularization. In such procedures, "*crossing*" of the occlusion with a guidewire is an essential step of the procedure as it would then be followed with a balloon catheter for angioplasty and possibly a stent. Despite the literature strongly suggesting that all peripheral arterial occlusions have either microchannels or soft penetrable segments [24], [25], however, it appears that conventional technologies fail in finding these penetrable sections. To test this hypothesis, and to compare the performance of the conventional technologies with the CathPilot, we created a phantom model that mimics the superior femoral artery (SFA) and has an occlusion at the distal end, as is shown in Fig. 10.

The SFA model was created from transparent and flexible polyvinyl chloride with an I.D. of 10 mm. A top view camera was used as image guidance to mimic X-ray fluoroscopy and to provide the user with image feedback.

To mimic the occlusion, we 3-D printed four lesions with holes of 1.25-mm diameter at distances of 0, 1.25, 3.75, and 5 mm from the center [representative occlusion shown in Fig. 10(a)]. The penetrable holes were embedded within an array of impenetrable dimples to better simulate a real heterogenous lesion. The performance of three methods in crossing the occlusion were compared: conventional nonsteerable catheter (GLIDECATH 4Fr, Terumois); steerable Catheter (DIREX 12Fr, Boston Scientific); and the CathPilot. All catheters were used to support and navigate a straight 0.035" or J-shaped guidewire (Glidewire, Terumois); the user was free to interchange the guidewire type as needed. Seven users (four novice users and three vascular interventionalists with varying levels of experience ranging from 1 to 15 years) were randomly assigned a lesions (from the batch of four printed lesions) and requested to perform five iterations. The lesion was positioned within the fixture at a random orientation. The users were blinded to the lesion type (i.e., target hole location) and its orientation. Each user attempted crossing the assigned lesion with each of the three methods; the methods were assigned in random order. The measured criteria were the success or failure rates in crossing the lesion and the crossing time when the crossing was successful. The maximum permitted time for crossing was 10 min. The navigation times were statistically compared using a repeated measure two-way analysis of variance (ANOVA) within PRISM (GraphPad).

TABLE I
ERROR SUMMARY

Expansion Size	Straight	S Bend	90° Bend	Combined
10 mm	0.183 $\pm$ 0.129mm ($n = 29$)	0.200 $\pm$ 0.143mm ($n = 30$)	0.226 $\pm$ 0.151mm ($n = 28$)	0.203 $\pm$ 0.141mm ($n = 87$)
12.5 mm	0.236 $\pm$ 0.130mm ($n = 30$)	0.295 $\pm$ 0.199mm ($n = 28$)	0.283 $\pm$ 0.179mm ($n = 29$)	0.271 $\pm$ 0.171mm ($n = 87$)
15 mm	0.297 $\pm$ 0.166mm ($n = 36$)	0.387 $\pm$ 0.184mm ($n = 43$)	0.453 $\pm$ 0.228mm ($n = 35$)	0.379 $\pm$ 0.202mm ($n = 114$)
17.5mm	0.336 $\pm$ 0.218mm ($n = 28$)	0.343 $\pm$ 0.243mm ($n = 28$)	0.365 $\pm$ 0.235mm ($n = 34$)	0.349 $\pm$ 0.231mm ($n = 90$)

IV. RESULTS

With different levels of expansion and different tortuous paths, the steering mechanism functioned as expected, allowing for remote teleoperation of the manipulator and steering of the device to the entire reachable workspace at each expanded size.

The measured average errors in position estimation of the end-effector, across all configurations (seen in training) and normalized to the expansion diameter, were $2.09 \pm 1.41\%$, $2.17 \pm 1.37\%$, $2.52 \pm 1.35\%$, and $1.99 \pm 1.32\%$ for the 10, 12.5, 15, and 17.5 mm expansions, correspondingly. A summary of the actual positional errors can be found in Table I. The worst-case error in position estimation was observed at the 15-mm expansion size; however, it was less than 7.23% of the frame expansion. The average error in all configurations was $2.2 \pm 1.37\%$. At untrained intermediate frame expansion sizes

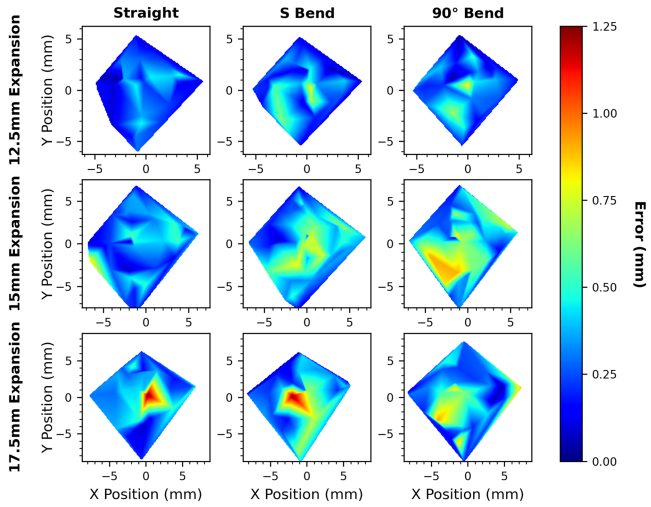

Fig. 11. Error heat maps of the estimated position of the device versus the actual measured position are shown for the CathPilot in three configurations: straight, S bend, and 90° bend.

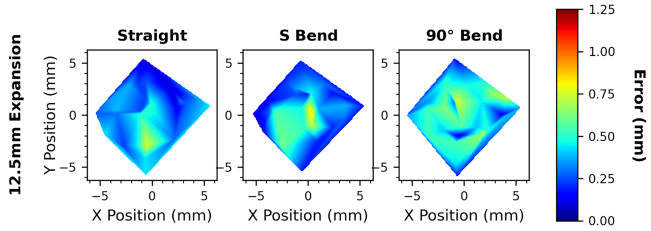

Fig. 12. Representative error heat map for configurations not seen by the trained position estimation method.

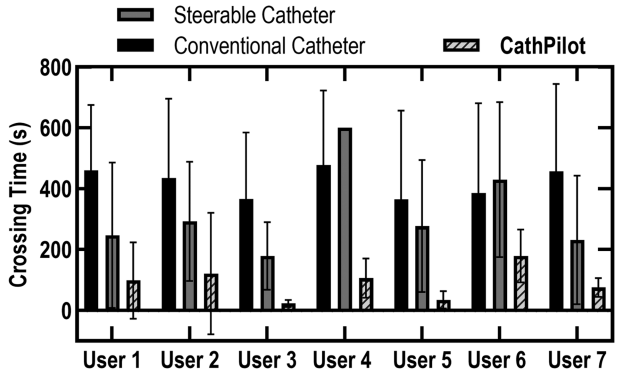

Fig. 13. Results of crossing time of five random lesions by seven users (blinded to lesion type) for each of the specified three methods are shown. The CathPilot was significantly faster in crossing ($p<0.0001$; two-way ANOVA). Note that User 4 failed with the steerable catheter in all cases within the allocated time (600 s) and, hence, there is no standard deviation for the corresponding bar.

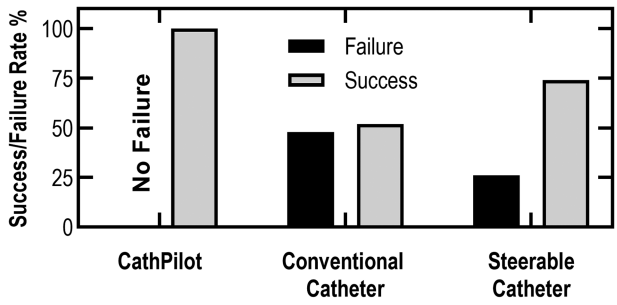

Fig. 14. Success versus failure counts of the crossing of the occlusion for the seven users using the three different navigation methods are shown. The users were always successful in finding the target with the CathPilot, whereas conventional methods sometimes failed.

of 11.25, 13.75, and 16.25 mm, the tracking error was 5.01± 2.2%, 3.5 ± 2.00, and 3.34 ± 1.92%, correspondingly. It is also important to understand the error at different locations of the workspace. The error heatmaps are shown in Fig. 10 (configurations seen by training dataset) and Fig. 11 (unseen configurations by training dataset). These heatmaps were created by linear interpolation between neighboring points using the ∼30 discrete points acquired at each testing condition.

At unseen configurations, the system maintained relative performance, as illustrated by Fig. 12, which shows the tracking performance for the various unseen configurations at a given representative expansion size of 12.5 mm. The measured average error in position estimation—for configurations not seen in the training—across all configurations and normalized to the expansion diameter were $2.77 \pm 1.80\%$, $2.90 \pm 1.49\%$, $3.33 \pm 1.76\%$, and $2.55 \pm 1.55\%$ for the 10, 12.5, 15, and 17.5 mm expansions, correspondingly.

The CathPilot design assumes the user would rely on the provided GUI [see Fig. 9(a)] and its corresponding tracking data for feedback and navigation, which utilize cable length variations for position estimation, as previously described. However, to further analyze the system, the mapping error between the thumbstick and the end-effector was also measured. The average errors in the mapping between the thumbstick and the end-effector across all configurations and normalized to the expansion diameter were $7.02 \pm 2.71\%$, $6.89 \pm 3.47\%$, $7.78 \pm 3.76\%$, and $6.11 \pm 4.44\%$ for 10, 12.5, 15, and 17.5 mm expansion sizes, correspondingly.

The results of the phantom validation experiments show that the CathPilot led to a significantly faster crossing time ($p<0.0001$; two-way repeated measures ANOVA), as shown in Fig. 13. Also, while the conventional nonsteerable and steerable catheters sometimes failed in finding the penetrable segments of the occlusion and crossing them, the CathPilot was always successful in lesion crossing, as shown in Fig. 14.

V. Discussion

By utilizing the X-CADPAM concept, our proposed CathPilot system overcomes the limitations of conventional CADPAMs while taking advantage of their many benefits. The proposed approach allows us to reach target areas only accessible through narrow passageways (such as the vessel lumen) and permits us to accurately control the position of a device (e.g., a catheter or guidewire) anywhere within the expandable frame workspace while being able to track and visualize its position in real time with submillimeter accuracy.

Our experiments show that the CathPilot is capable of maintaining accurate position control and tracking with a mean error below 2.2% of the workspace size, which was 10–20 mm in diameter in our prototype, regardless of the test path tortuosity and catheter shape for all trained expansion sizes. For intermediate untrained expansion sizes, the worst-case error was below 5.01% of the expansion size. However, in future, this can be mitigated by including training sets that include more expansion sizes for training. We believe the current submillimeter accuracy is sufficient for most potential clinical indications of use, particularly in cardiovascular interventions. As a supporting example, the reported positioning errors are on the same order as that of a small-sized 0.014" (0.35 mm) guidewire that is generally the smallest diameter device used by cardiovascular interventionalists.

As previously mentioned, cardiovascular interventions are also limited by conventional X-ray fluoroscopy guidance as it only provides 2-D projection images and lack depth information. The proposed CathPilot addresses this limitation by providing the user with graphic visual feedback showing the relative position of the end-effector in the axial plane, in real time. Combined with the X-ray fluoroscopy (that provides 2-D information), we can provide the user with complete 3-D feedback and image guidance.

The CathPilot system presented in this article was designed for a 12 Fr size delivery sheath. While this size is sufficiently small for various indications of use in applications, such as in electrophysiology, structural heart procedures, or aortic repair, various other applications require smaller diameter devices. Our current prototype was limited in miniaturization as we were using NiTi wires and welding them to generate the desired frame shape, however, for future work, we plan to further miniaturize the size of the system by laser-cutting thin-walled NiTi tubes and then forming them to shape to create the frame similar to that of stent manufacturing.

While the proposed system provides a high level of accuracy in device position estimation, however, several of the simplifying assumptions may be further improved as part of future work. Specifically, it was assumed that the expandable frame was expanded symmetrically. While we believe in practice this will be a reasonable assumption, the system must be tested within various anatomical environments with asymmetric geometrical constraints to further validate this assumption and to develop corresponding position estimation methods if the current methods are insufficient. One approach could be to utilize the tension of the cables, together with a quasi-static model of the frame to predict the frame shape. Furthermore, at longer lengths of the device, the friction of the cable/channel may accumulate and also the vibration and elasticity of the cables may no longer be negligible depending on the length of the system. Another simplifying assumption was a 2-D workspace for the end-effector. These challenges deserve further attention and analysis as part of future studies.

We believe this novel technology will have a wide range of applications where access to the site is limited to a narrow and tortuous passageway. Our target initial indications of use are for minimally invasive catheter-based procedures. For these interventions, the proposed system does not disrupt the procedure flow as it is designed and operated similar to a conventional steerable catheter [12]. Furthermore, the direct mapping between the user thumbstick (at the input handle) and the end-effector motion at the manipulator promises an ergonomic and intuitive user interface, with intrinsic haptic feedback. As part of future studies, we plan to explore the safety and efficacy of the proposed system for multiple minimally invasive procedures. Furthermore, we plan to explore other potential applications of this technology in applications where access to the target site is limited to a long, narrow, and tortuous path.

VI. Conclusion

The CathPilot system described in this article is capable of navigating through a narrow, long, and tortuous passageway and provides the user with full remote control over the device's position within the workspace of the CathPilot's expanded frame relative to the anatomy. The system provides real-time device position tracking with a mean error below 2.2% of the workspace size. When used in combination with conventional X-ray fluoroscopy, the system allows the user to accurately visualize the device position in 3-D relative to the anatomy. The system is fully passive, mechanically operated, allows for a direct mapping between the user-operated input handle and the device position, and provides haptic feedback. This device promises to overcome many of the limitations and challenges associated with steering and navigation of conventional interventional devices and can potentially greatly improve the efficiency and outcome of the corresponding procedures.

Acknowledgment

The authors would like to thank the funding agencies for their support of this project, as well as Michael Pozzobon, Dr. T. Roy, Dr. B. V. Asseldonk, team at Magellan Biomedical Inc., Toronto Metropolitan University, and the Sunnybrook Research Institute for their continued support.

References

[1] G. A. Roth et al., "Global, regional, and national burden of cardiovascular diseases for 10 causes, 1990 to 2015," *J. Amer. College Cardiol.*, vol. 70, no. 1, pp. 1–25, Jul. 2017.

[2] N. J. Kassebaum et al., "Global, regional, and national disability-adjusted life-years (DALYs) for 315 diseases and injuries and healthy life expectancy (HALE), 1990–2015: A systematic analysis for the global burden of disease study 2015," *Lancet*, vol. 388, no. 10053, pp. 1603–1658, Oct. 2016.

[3] H. S. Lisboa, "Cardiovascular 2019," 2019. Accessed: Jun. 8, 2021. [Online]. Available: https://cardiovascular.cardiologymeeting.com/2019

[4] A. W. Bradbury et al., "Bypass versus angioplasty in severe ischaemia of the leg (BASIL) trial: An intention-to-treat analysis of amputation-free and overall survival in patients randomized to a bypass surgery-first or a balloon angioplasty-first revascularization strategy," *J. Vasc. Surg.*, vol. 51, no. 5 SUPPL, pp. 5S–17S, 2010.

[5] J. C. Hsu et al., "Randomized trial of conventional transseptal needle versus radiofrequency energy needle puncture for left atrial access (the TRAVERSE-LA study)," *J. Amer. Heart Assoc.*, vol. 2, no. 5, 2013, Art. no. e000428.

[6] M. A. Al-Hijji et al., "Trends and predictors of repeat catheter ablation for atrial fibrillation," *Amer. Heart J.*, vol. 171, no. 1, pp. 48–55, Jan. 2016.

[7] A. Gupta et al., "Complications of catheter ablation of atrial fibrillation a systematic review," *Circulation: Arrhythmia Electrophysiol.*, vol. 6, no. 6, pp. 1082–1088, Dec. 2013.
[8] D. Daye and T. G. Walker, "Complications of endovascular aneurysm repair of the thoracic and abdominal aorta: Evaluation and management," *Cardiovasc. Diagnosis Ther.*, vol. 8, no. Suppl 1, pp. S138–S156, Apr. 2018.
[9] E. S. Brilakis et al., "Procedural outcomes of chronic total occlusion percutaneous coronary intervention: A report from the NCDR (National Cardiovascular Data Registry)," *JACC: Cardiovasc. Interv.*, vol. 8, no. 2, pp. 245–253, Feb. 2015.
[10] A. Ali et al., "Catheter steering in interventional cardiology: Mechanical analysis and novel solution," *Proc. Inst. Mech. Engineers, Part H, J. Eng. Med.*, vol. 233, no. 12, pp. 1207–1218, Dec. 2019.
[11] A. Ali, D. H. Plettenburg, and P. Breedveld, "Steerable catheters in cardiology: Classifying steerability and assessing future challenges," *IEEE Trans. Biomed. Eng.*, vol. 63, no. 4, pp. 679–693, Apr. 2016.
[12] X. Hu, A. Chen, Y. Luo, C. Zhang, and E. Zhang, "Steerable catheters for minimally invasive surgery: A review and future directions," *Comput. Assist. Surg.*, vol. 23, no. 1, pp. 21–41, Jan. 2018.
[13] T. L. Roy, M. A. Tavallaei, J. J. Zhou, and A. D. Dueck, "Performance assessment of a novel steering catheter for crossing peripheral arterial occlusions," *J. Vasc. Surg.*, vol. 70, no. 4, Oct. 2019, Art. no. e100.
[14] E. Gallitto et al., "Impact of iliac artery anatomy on the outcome of fenestrated and branched endovascular aortic repair," *J. Vasc. Surg.*, vol. 66, no. 6, pp. 1659–1667, Dec. 2017.
[15] E. Gallitto et al., "Steerable sheath for cannulation and bridging stenting of challenging target visceral vessels in fenestrated and branched endografting," *Ann. Vasc. Surg.*, vol. 67, pp. 26–34, Aug. 2020.
[16] B. O'Brien, H. Zafar, S. De Freitas, and F. Sharif, "Transseptal puncture—Review of anatomy, techniques, complications and challenges," *Int. J. Cardiol.*, vol. 233, pp. 12–22, Apr. 2017.
[17] S. Sahoo, T. Kariya, and K. Ishikawa, "Targeted delivery of therapeutic agents to the heart," *Nat. Rev. Cardiol.*, vol. 18, no. 6, pp. 389–399, Jan. 2021.
[18] W. Sherman, T. P. Martens, J. F. Viles-Gonzalez, and T. Siminiak, "Catheter-based delivery of cells to the heart," *Nat. Clin. Pract. Cardiovasc. Med.*, vol. 3, no. S1, pp. S57–S64, Mar. 2006.
[19] M. A. Allison et al., "Ethnic-specific prevalence of peripheral arterial disease in the United States," *Amer. J. Prev. Med.*, vol. 32, no. 4, pp. 328–333, Apr. 2007.
[20] M. Lovell et al., "Peripheral arterial disease: Lack of awareness in Canada," *Can. J. Cardiol.*, vol. 25, no. 1, pp. 39–45, Jan. 2009.
[21] Y. H. Qiu et al., "Determination of risk factors and establishment of a prediction model for immediate technical failure during endovascular treatment of femoropopliteal occlusive disease," *Ann. Vasc. Surg.*, vol. 48, pp. 35–44, Apr. 2018.
[22] J. A. Gutierrez and M. R. Patel, "Crossing peripheral chronic total occlusions: More tolls and more questions," *J. Amer. Heart Assoc.*, vol. 10, no. 20, Oct. 2021, Art. no. 23423.
[23] T. Roy, T. Forbes, G. Wright, and A. Dueck, "Burning bridges: Mechanisms and implications of endovascular failure in the treatment of peripheral artery disease," *J. Endovascular Ther.*, vol. 22, no. 6, pp. 874–880, Dec. 2015.
[24] N. R. Munce et al., "Ex vivo imaging of chronic total occlusions using forward-looking optical coherence tomography," *Lasers Surg. Med.*, vol. 39, no. 1, pp. 28–35, Jan. 2007.
[25] T. Roy, G. Liu, N. Shaikh, A. D. Dueck, and G. A. Wright, "Puncturing plaques," *J. Endovascular Ther.*, vol. 24, no. 1, pp. 35–46, Feb. 2017.
[26] H. Rafii-Tari, C. J. Payne, and G. Z. Yang, "Current and emerging robot-assisted endovascular catheterization technologies: A review," *Ann. Biomed. Eng.*, vol. 42, no. 4, pp. 697–715, 2014.
[27] T. da Veiga et al., "Challenges of continuum robots in clinical context: A review," *Prog. Biomed. Eng.*, vol. 2, no. 3, Aug. 2020, Art. no. 032003.
[28] J. Burgner-Kahrs, D. C. Rucker, and H. Choset, "Continuum robots for medical applications: A survey," *IEEE Trans. Robot.*, vol. 31, no. 6, pp. 1261–1280, Dec. 2015.
[29] F. Kiemeneij, M. S. Patterson, G. Amoroso, G. Laarman, and T. Slagboom, "Use of the Stereotaxis Niobe magnetic navigation system for percutaneous coronary intervention: Results from 350 consecutive patients," *Catheterization Cardiovasc. Interv.*, vol. 71, no. 4, pp. 510–516, Mar. 2008.
[30] J. Hwang, J. Kim, and H. Choi, "A review of magnetic actuation systems and magnetically actuated guidewire- and catheter-based microrobots for vascular interventions," *Intell. Service Robot.*, vol. 13, no. 1, pp. 1–14, Jan. 2020.
[31] C. Shi et al., "Shape sensing techniques for continuum robots in minimally invasive surgery: A survey," *IEEE Trans. Biomed. Eng.*, vol. 64, no. 8, pp. 1665–1678, Aug. 2017.
[32] A. M. Franz, T. Haidegger, W. Birkfellner, K. Cleary, T. M. Peters, and L. Maier-Hein, "Electromagnetic tracking in medicine—A review of technology, validation, and applications," *IEEE Trans. Med. Imag.*, vol. 33, no. 8, pp. 1702–1725, Aug. 2014.
[33] M. Miyasaka, M. Haghighipanah, Y. Li, J. Matheson, A. Lewis, and B. Hannaford, "Modeling cable-driven robot with hysteresis and cable-pulley network friction," *IEEE/ASME Trans. Mechatronics*, vol. 25, no. 2, pp. 1095–1104, Apr. 2020.
[34] H. Jamshidifar, A. Khajepour, B. Fidan, and M. Rushton, "Vibration regulation of kinematically constrained cable-driven parallel robots with minimum number of actuators," *IEEE/ASME Trans. Mechatronics*, vol. 25, no. 1, pp. 21–31, Feb. 2020.
[35] H. Wang, J. Kinugawa, and K. Kosuge, "Exact kinematic modeling and identification of reconfigurable cable-driven robots with dual-pulley cable guiding mechanisms," *IEEE/ASME Trans. Mechatronics*, vol. 24, no. 2, pp. 774–784, Apr. 2019.
[36] T. Bruckmann, L. Mikelsons, T. Brandt, M. Hiller, and D. Schramm, "Wire robots part I: Kinematics, analysis & design," in *Parallel Manipulators, New Developments*. London, UK: I-Tech Education and Publishing, 2008.
[37] M. Runciman, J. Avery, M. Zhao, A. Darzi, and G. P. Mylonas, "Deployable, variable stiffness, cable driven robot for minimally invasive surgery," *Front. Robot. AI*, vol. 6, Jan. 2020, Art. no. 141.
[38] T. J. C. O. Vrielink, M. Zhao, A. Darzi, and G. P. Mylonas, "ESD CYCLOPS: A new robotic surgical system for GI surgery," in *Proc. IEEE Int. Conf. Robot. Autom.*, Sep. 2018, pp. 150–157.
[39] G. Mylonas, V. Vitiello, T. P. Cundy, A. Darzi, and G.-Z. Yang, "CYCLOPS: A versatile robotic tool for bimanual single-access and natural-orifice endoscopic surgery," in *Proc. IEEE Int. Conf. Robot. Automat.*, 2014, pp. 2436–2442.
[40] "scikit-learn: Machine learning in Python— Scikit-learn 0.24.2 documentation," Apr. 2021. Accessed: Jun. 13, 2021. [Online]. Available: https://scikit-learn.org/stable/

James J. Zhou received the BA.Sc. in mechanical engineering (undergraduate degree) with specialization in biomechanics from the University of Waterloo, Waterloo, ON, Canada, in 2019, and the M.Sc. degree in biomedical engineering from Toronto Metropolitan University (TMU), in 2021.

He is currently a Research and Development Engineer with Medtronic, Dublin, Ireland.

Amaar Quadri is currently a senior undergraduate student in mechanical engineering with the University of Waterloo, Waterloo, ON, Canada.

He has been a Research Assistant with MD-SLab, Toronto Metropolitan University, Toronto, ON, Canada. His research interests include mathematical and mechanical design, modeling, programming, and mechatronics R&D.

Alykhan Sewani (Member, IEEE) received the BA.Sc. in mechanical engineering from University of Waterloo, Waterloo, ON, Canada with specialization in biomechanics, in 2019. He is currently working toward the M.Sc. degree in biomedical engineering with Toronto Metropolitan University (TMU), Toronto, ON, Canada.

His research focuses on developing new ultrasound imaging instruments for cardiovascular interventions.

Yara Alawneh received the undergraduate degree in biomedical engineering from Toronto Metropolitan University, Toronto, ON, Canada, in 2020. She is currently working toward the M.Sc. degree in biomedical engineering with Toronto Metropolitan University, Toronto, ON, Canada.

Her research focuses on developing new solutions to improve minimally invasive cardiovascular procedures.

Rene Gilliland-Rocque is currently a senior undergraduate student in the BME program with Toronto Metropolitan University (TMU) , Toronto, ON, Canada.

He has been a Research Assistant with the MDSLab, TMU. His research interests include various electromechanical hardware designs and development.

Christopher Magnin received the undergraduate degree in biomedical engineering from Vanderbil University, Nashville, TN, USA, and the M.Sc. degree in engineering management from Duke University, Durham, NC, USA.

He has more than 15 years of experience in medical device design and development and is currently a Consulting Engineer for Magellan Biomedical, Richmond Hill, ON, Canada.

Andrew Dueck received the B.Sc. in cell/cellular and molecular biology from the University of Waterloo, and the M.Sc. degree in clinical epidemiology from the University of Toronto, Toronto, ON, Canada, and the MD from Queen's University. He completed his residency in General Surgery, as well as his fellowship in vascular surgery with the University of Toronto, Toronto, ON, Canada.

He is an Assistant Professor of Surgery with the University of Toronto and Vascular and Endovascular surgeon with the Schulich Heart Centre, Sunnybrook Health Sciences Centre, Toronto, ON, Canada.

Graham A. Wright received his Ph.D. degree in electrical engineering from Stanford University, Stanford, CA, USA, in 1991.

He is currently a Senior Scientist with the Sunnybrook Health Sciences Centre, Toronto, ON, Canada, and a Professor with the Department of Medical Physics, University of Toronto, Toronto, ON, Canada. He has been appointed the Canada Research Chair in Imaging for Cardiovascular Therapeutics since 2010.

M. Ali Tavallaei (Member, IEEE) received the Ph.D. degree in biomedical engineering from Western University, London, ON, Canada, in 2015.

He is currently a Canada Research Chair in systems and devices for cardiovascular interventions and an Assistant Professor with the Department of ECBE, Toronto Metropolitan University, Toronto, ON, Canada. He is also a Visiting Scientist with Sunnybrook, Toronto, ON, Canada, an Assistant Professor (status-only) with the Department of ECE, University of Toronto, Toronto, ON, Canada, and a Scientist with the Keenan Research Centre.